Electronic Supplementary Information (ESI) for

Achieving Narrowband Deep-Blue Electroluminescence (CIE y = 0.04) via a Fluorinated and Sterically Modulated MR-TADF Emitter

Haiping Wen, Ziyan Zhao, Rujia Yuan, Qiuqi Wang, Huiqi Xie, and Yingyuan Hu*

Contents

1. Materials and instruments

All chemicals and reagents were purchased from commercial sources and used as received without further purification. Vacuum sublimation was applied to the final compound prior to photophysical (PL) and electroluminescence (EL) investigations. ^{1}H and ^{13}C NMR spectra were recorded on an AVABCEIII spectrometer in $CDCl_3$ at room temperature. High-resolution mass spectra (HRMS) were acquired on a Waters G2-S QTof mass spectrometer equipped with an electrospray ionization (ESI) source. Sample purity test was performed on an Agilent 1260 HPLC system with DAD detector, detection wavelength 280 nm and flow rate 0.600 mL/min. Thermogravimetric analysis (TGA) was performed on a NETZSCH TG 209F1 Libra under nitrogen at a heating rate of 20.0 K min^{-1}. UV-vis absorption spectra were measured on a Shimadzu UV-3600 spectrophotometer. Steady-state PL spectra were recorded on a Horiba Fluoromax-4 spectrofluorometer, and absolute PL quantum yields were determined using a Hamamatsu C11347 Quantaurus_QY system. Transient PL decay measurements were carried out using an Edinburgh FLS1000 fluorescence lifetime system, with spectra collected under nitrogen atmosphere under vacuum for films. Low-temperature fluorescence and phosphorescence spectra were recorded at 77 K using a 5 wt% 4FBN-Me:mCBP doped film. Cyclic voltammetry (CV) measurements were conducted in dichloromethane (DCM) containing 0.1 M tetrabutylammonium hexafluorophosphate ($TBAPF_6$) with a scan rate of 100 mV s^{-1}, using a three-electrode setup consisting of an Ag/AgCl reference electrode, a Pt-C working electrode, and a Pt wire counter electrode. Ferrocene (Fc) was used as an internal standard and all potentials were calibrated against the Fc/Fc^{+} redox couple. Ground-state DFT and excited-state TD-DFT calculations were carried out using Gaussian 16. Geometry optimizations were performed at the B3LYP/6-31G** level, and harmonic frequency analyses at the same level confirmed the optimized structures as true minima. Vertical excitation energies were obtained by TD-DFT using the B3LYP/6-31G** level on the optimized geometries. Spin–orbit coupling (SOC) matrix elements between the relevant singlet

and triplet excited states were computed with ORCA using the same B3LYP/6-31G** level of theory on the corresponding optimized geometries.

2. OLED fabrication and characterization

The glass substrates precoated with a 90-nm layer of indium tin oxide (ITO) with a sheet resistance of 15~20 Ω per square were successively cleaned in ultrasonic bath of acetone, isopropanol, detergent and deionized water, respectively, taking 10 minutes for each step. Then, the substrates were totally dried in a 70 ^{o}C oven. Before the fabrication processes, in order to improve the hole injection ability of ITO, the substrates were treated by O_2 plasma for 10 minutes. The vacuum-deposited OLEDs were fabricated under a pressure of $< 1 \times 10^{-5}$ Pa. Organic materials were purified by vacuum sublimation before use, and the reported performance values are representative. Organic materials, LiF and Al were deposited at rates of 1~2 A s^{-1}, 0.1 A s^{-1} and 4 A s^{-1}, respectively. The effective emitting area of the devices is 9 mm^2, determined by the overlap between anode and cathode. The EL spectra, luminance-voltage-current density and external quantum efficiency were characterized with a dual-channel Keithley 2400 source meter and a PR-670 spectrometer. The external quantum efficiencies were estimated utilizing the normalized EL spectra and the current efficiencies of the devices, assuming that the devices are Lambertian emitters. All the characterizations were conducted at room temperature in ambient conditions without any encapsulation.

3. Estimation of photophysical parameters

In this study, the prompt fluorescent component (Φ_p) and delayed fluorescent component (Φ_d) of PLQY can be distinguished from the total PLQY (Φ) by comparing the integrated intensities of the prompt and delayed components in the transient photoluminescence spectra.[1, 2]

Rate constants (k_r, k_{nr}, k_{ISC}, and k_{RISC}) were determined from the measurements of quantum yields (Φ_p and Φ_d) and lifetimes (τ_p, τ_d) and of the prompt (fluorescence) and delayed (TADF) components according to equations 1-6.[3, 4]

Where τ_p and τ_d represent the prompt and delayed fluorescence lifetime, Φ is the total fluorescence quantum yield. The Φ_p is the prompt fluorescent component of Φ_{PL}. The Φ_d is the delayed fluorescent component of Φ. The k_p and k_d represent the decay rate constants for prompt and delayed fluorescence, respectively. The k_r is the rate constant of radiative decay, and the $k$nr is the rate constant of nonradiative decay. The k_{ISC} and k_{RISC} are the rate constants of intersystem crossing and reverse intersystem crossing, respectively.

Estimation of the rate constants of 5 wt% mCBP-doped film based on 4FBN-Me at 300K.

$\Phi = 0.758$

$\Phi_p = 0.3552$

$\Phi_d = 0.4028$

$\tau_p = 5.72$ ns

$\tau_d = 9.19$ μs

$k_p = 1.75 \times 10^8\ s^{-1}$ $\quad k_p = 1/\tau_p$ (1)

$k_d = 1.09 \times 10^5\ s^{-1}$ $\quad k_d = 1/\tau_d$ (2)

$k_r = 6.21 \times 10^7\ s^{-1}$ $\quad k_r = \Phi_p k_p + \Phi_d k_d$ (3)

$k_{nr} = 1.98 \times 10^7\ s^{-1}$ $\quad k_{nr} = (1-\Phi)k_r/\Phi$ (4)

$k_{ISC} = 9.28 \times 10^7\ s^{-1}$ $\quad k_{ISC} = k_p - k_r - k_{nr}$ (5)

k_{RISC} =2.32 × 10^5 s^{-1} $k_{RISC} = (k_p \cdot k_d \cdot \Phi_d)/(k_{ISC} \cdot \Phi_p)$ (6)

Table. S1. The detailed data of temperature-dependent transient PL decay spectra of 4FBN-Me in doped films.

Compound	T (K)	⟨τ⟩ (μs)	$\tau_{delayed}$ (ns)	$R_{delayed}$ (%)
4FBN-Me	300	5.22	9191.08	53.14
	200	3.21	9628.86	28.55
	100	2.07	11585.73	13.50

4. Synthesis and characterization

N1,N3-bis(2,6-difluorophenyl)-5-methylbenzene-1,3-diamine(M_1): To a solution of 1,3-dibromo-5-methylbenzene (1g, 4.00mmol), 2,6-difluoroaniline (1.14g, 8.80mmol) and sodium tert-butoxide (1.15g, 12.00 mmol) in toluene (20 mL) were added XPhos (76.3mg ,0.16mmol). After purging with nitrogen for 10minutes, $Pd_2(dba)_3$ (73.3 mg, 0.08 mmol) was added and nitrogen purging continue for 10minutes. Then after stirring at 100 ºC for 10 h, the reaction mixture was cooled to room temperature and diluted with CH_2Cl_2. The mixture was filtered through silicagel and concentrated. After concentration, the residue was purified by using column chromatography (DCM/Hexane). The resulting residue was dried at 50 ºC under vacuum to give the desired product (1.21g, 87%) as a paste. ^{1}H NMR (400 MHz, $CDCl_3$) δ 7.07-6.89 (m, 6H), 6.20 (d, J = 2.1 Hz, 2H), 6.08 (s, 1H), 5.36 (s, 2H), 2.23 (s, 3H). ^{13}C NMR (101 MHz, $CDCl_3$) δ 158.24, 158.18, 155.78, 155.72, 144.63, 139.86, 123.60, 123.50, 123.41, 119.59, 119.44, 119.28, 112.05, 111.99, 111.88, 111.82, 109.41, 100.95, 21.80.

N1,N3-bis(2,6-difluorophenyl)-5-methyl-N1,N3-diphenylbenzene-1,3-diamine (M_2)：To a solution of M_1 (1g, 2.89 mmol), bromobenzene (0.99g, 6.35 mmol) and sodium tert-butoxide (1.11g, 11.55 mmol) in toluene (20 mL) were added XPhos (137.6mg ,0.29mmol). After purging with nitrogen for 10minutes, $Pd_2(dba)_3$ (128.2 mg, 0.14 mmol) was added and nitrogen purging continue for 10minutes. Then after stirring at 100 ºC for 16 h, the reaction mixture was cooled to room temperature and diluted with CH_2Cl_2. The mixture was filtered through silicagel and concentrated. After concentration, the residue was purified by using

column chromatography (DCM/Hexane). The resulting residue was dried at 50 ºC under vacuum to give the desired product (0.95g, 66%) as white solid. ^{1}H NMR (400 MHz, $CDCl_3$) δ 7.24-7.11 (m, 6H), 7.02-6.87 (m, 10H), 6.56 (s, 1H), 6.44 (s, 2H), 2.16 (s, 3H). ^{13}C NMR (101 MHz, $CDCl_3$) δ 161.84, 161.79, 159.33, 159.28, 147.09, 146.34, 139.93, 129.14, 127.12, 127.01, 126.92, 122.99, 122.85, 122.70, 122.42, 122.39, 121.06, 121.03, 116.12, 112.75, 112.70, 112.57, 112.51, 111.63, 21.82.

5,9-bis(2,6-difluorophenyl)-7-methyl-5,9-dihydro-5,9-diaza-13b-boranaphtho[3,2,1-de]anthracene (4FBN-Me) : To a solution of M_2(0.8g, 1.60 mmol) in 1,2-dichlorobenzene (20 mL) were added boron tribromide (0.59 mL,6.20 mmol) under nitrogen atmosphere at room temperature. After stirring at 210 ºC for 18hours, the reaction mixture were allowed to cool to room temperature. Then solvent were removed in vacuo, then residue was dissolved in toluene. The mixture was filtered through silicagel and concentrated. After concentration, the residue was purified by using column chromatography (DCM/Hexane). The resulting residue was dried at 50 ºC under vacuum to give the desired product (578 mg, 71%) as yellow solid. ^{1}H NMR (400 MHz, $CDCl_3$) δ 8.94 (dd, J = 7.7, 1.6 Hz, 2H), 7.60 (tt, J = 8.5, 6.1 Hz, 2H), 7.50 (ddd, J = 8.7, 7.0, 1.7 Hz, 2H), 7.35-7.26 (m, 5H), 7.25 (s, 1H), 6.79 (dd, J = 8.6, 1.2 Hz, 2H), 6.11 (s, 2H), 2.25 (s, 3H). ^{13}C NMR (101 MHz, $CDCl_3$) δ 161.98, 161.93, 159.44, 159.40, 146.59, 145.97, 144.13, 135.57, 131.82, 130.86, 130.76, 130.67, 120.89, 118.95, 118.78, 118.62, 115.26, 113.56, 113.54, 113.52, 113.38, 113.35, 113.33, 105.54, 23.33. HRMS (ESI-TOF) m/z: $[M+H]^+$ calcd for $C_{31}H_{20}BN_2F_4$ 507.1650; found 507.1659.

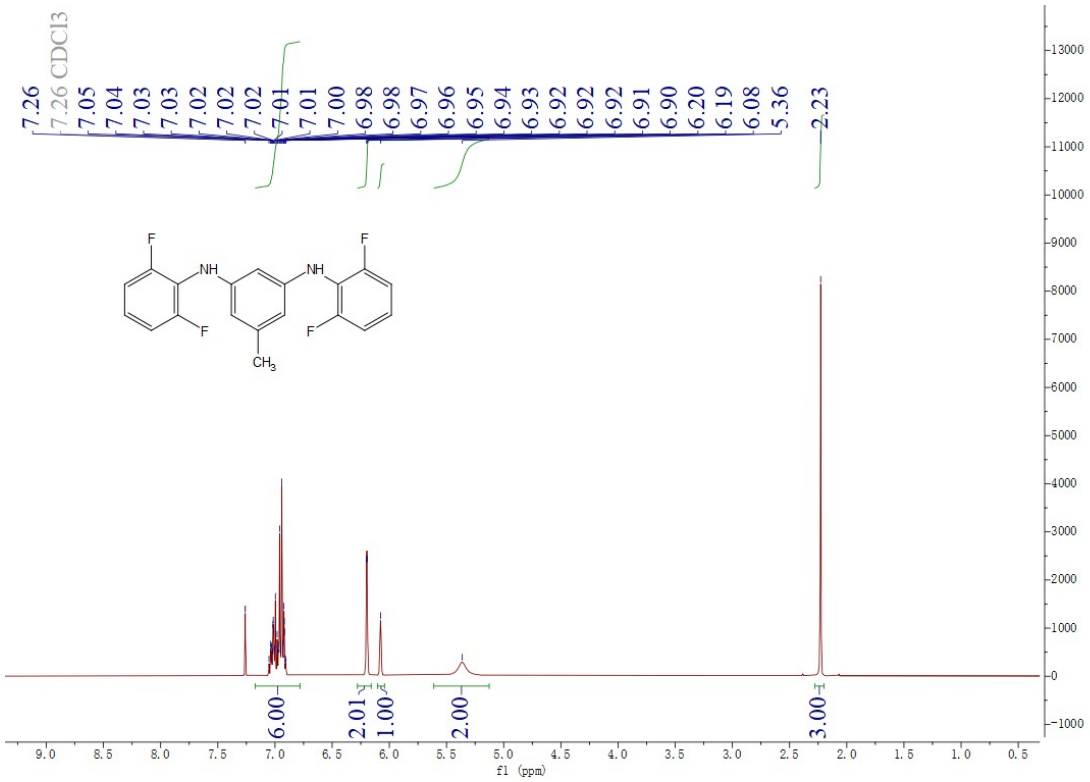

5. Supplementary figures and tables

Fig. S1 ^{1}H NMR spectra of M_1 in $CDCl_3$.

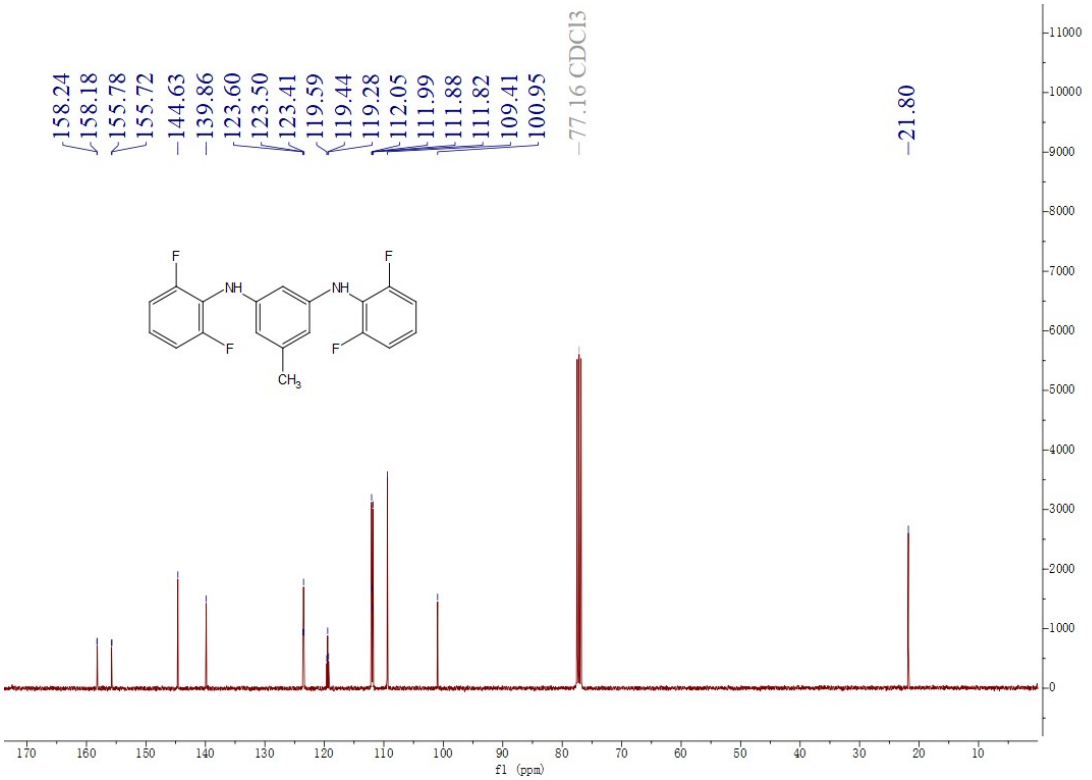

Fig. S2 ^{13}C NMR spectra of M_1 in $CDCl_3$.

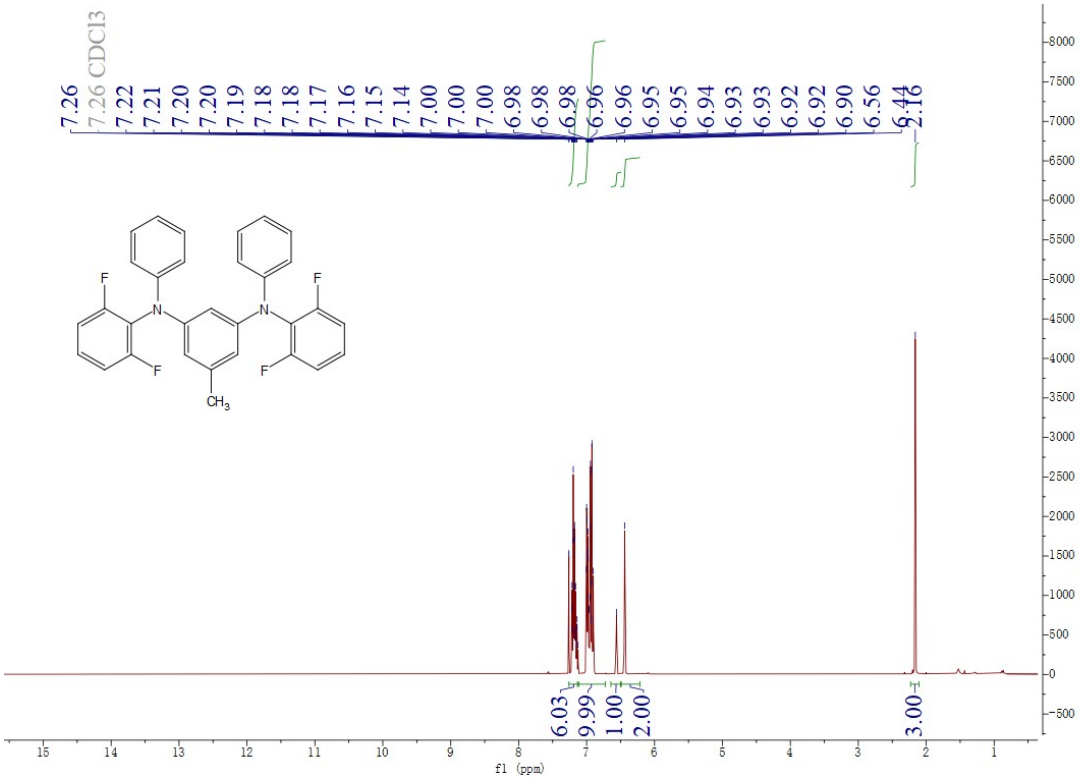

Fig. S3 ^{1}H NMR spectra of M_2 in $CDCl_3$.

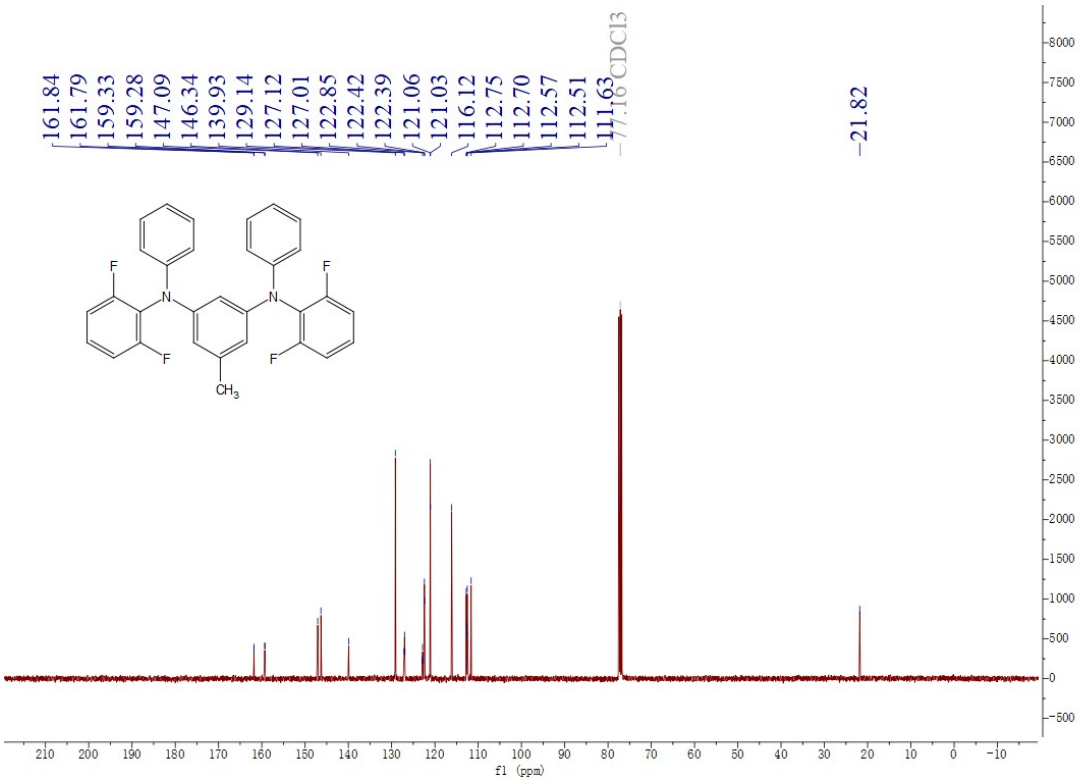

Fig. S4 ^{13}C NMR spectra of M_2 in $CDCl_3$.

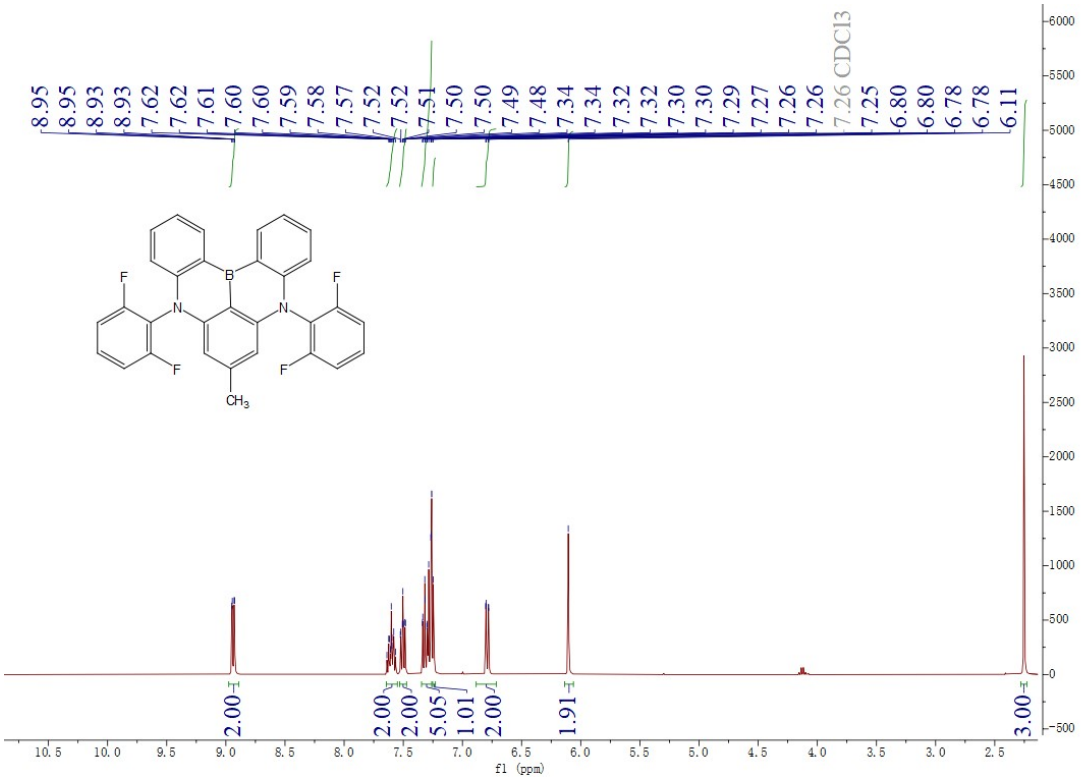

Fig. S5 ^{1}H NMR spectra of 4FBN-Me in $CDCl_3$.

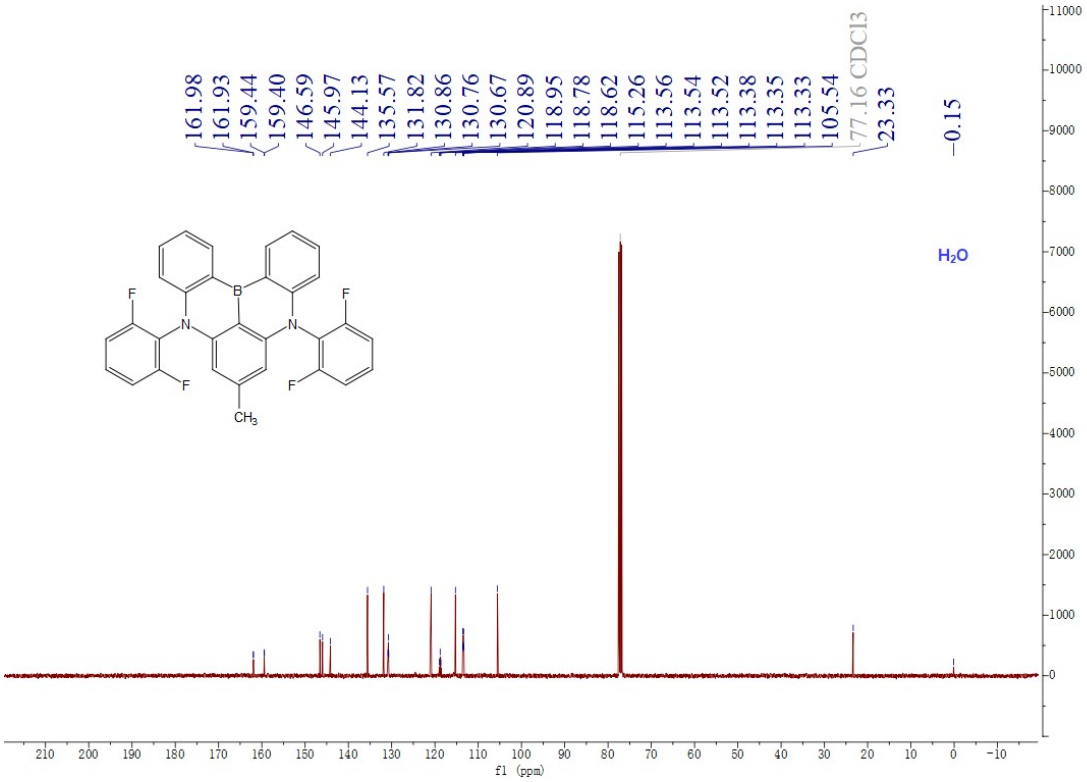

Fig. S6 ^{13}C NMR spectra of 4FBN-Me in $CDCl_3$.

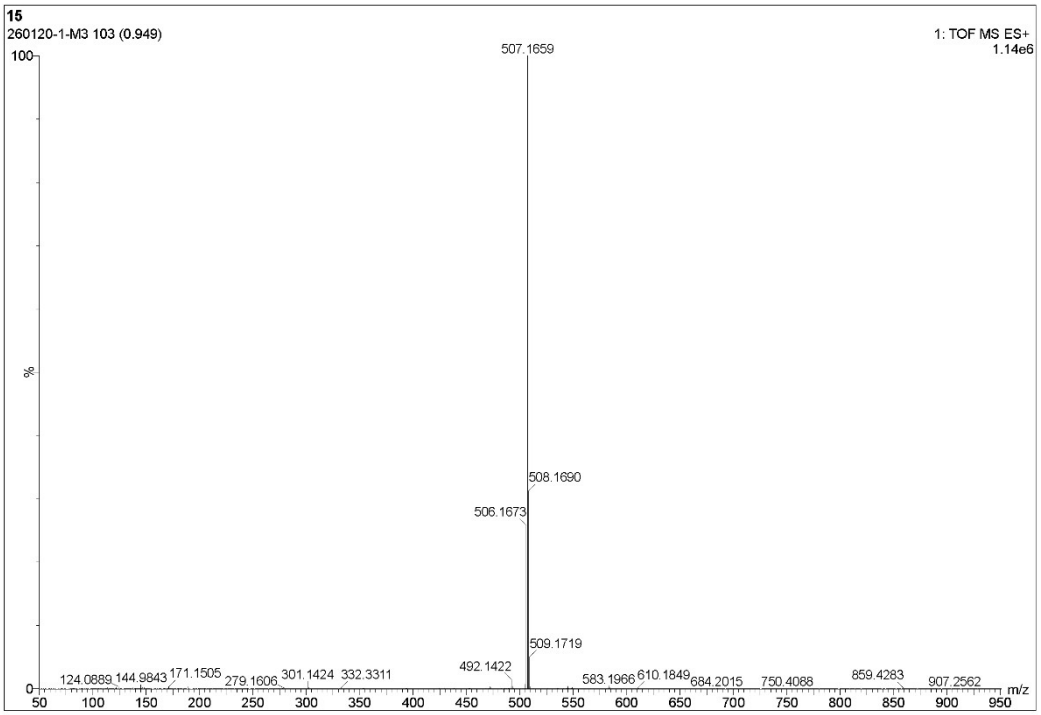

Fig. S7 High-resolution mass spectrometry of 4FBN-Me

Data File C:\CHEM32\1\DATA\WHP\20250406002653.D
Sample Name: 100

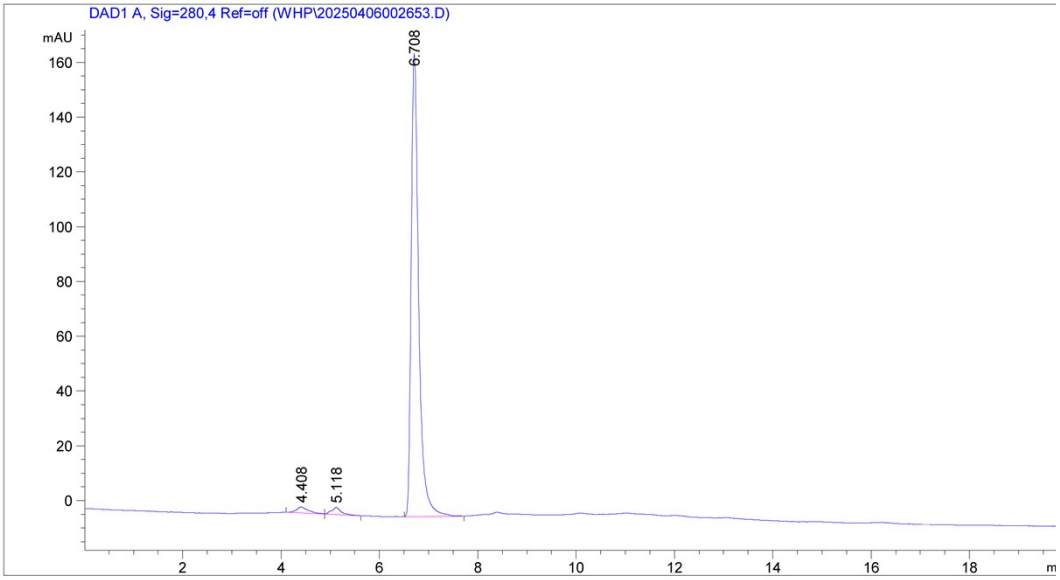


```
=====================================================================
                        Area Percent Report
=====================================================================

Sorted By             :      Signal
Multiplier            :      1.0000
Dilution              :      1.0000
Sample Amount:                :      1.00000  [ng/ul]   (not used in calc.)
Do not use Multiplier & Dilution Factor with ISTDs


Signal 1: DAD1 A, Sig=280,4 Ref=off

Peak RetTime Type  Width     Area      Height     Area
  #   [min]        [min]   [mAU*s]     [mAU]       %
----|-------|----|-------|----------|----------|--------|
   1   4.408 BB    0.2332    7.18611    0.42031   0.3980
   2   5.118 BB    0.1851    7.01328    0.51412   0.3884
   3   6.708 BB    0.1594 1791.42432  169.31586  99.2136

Totals :                  1805.62371  170.25029


=====================================================================
```

Fig. S8 HPLC chromatogram of 4FBN-Me, confirming a purity of 99.2%.

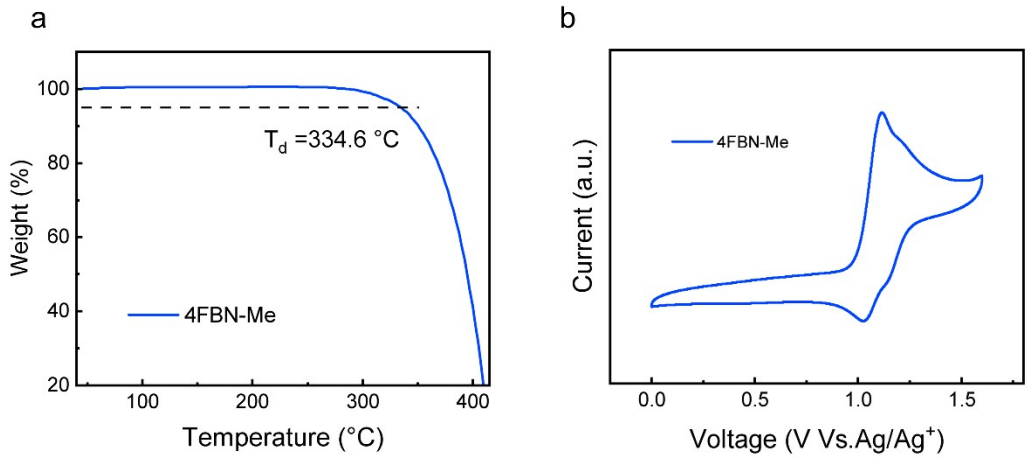

Fig. S9 (a) Cyclic voltammogram of 4FBN-Me measured in DCM containing 0.1 M tetra-n-butylammonium hexafluorophosphate ($TBAPF_6$ at a scan rate of 100 mV s^{-1} (reference electrode: Ag/AgCl). (b)Thermogravimetric analysis (TGA) curve of 4FBN-Me (T_d = 334.6 °C, 5% weight loss) recorded under nitrogen.

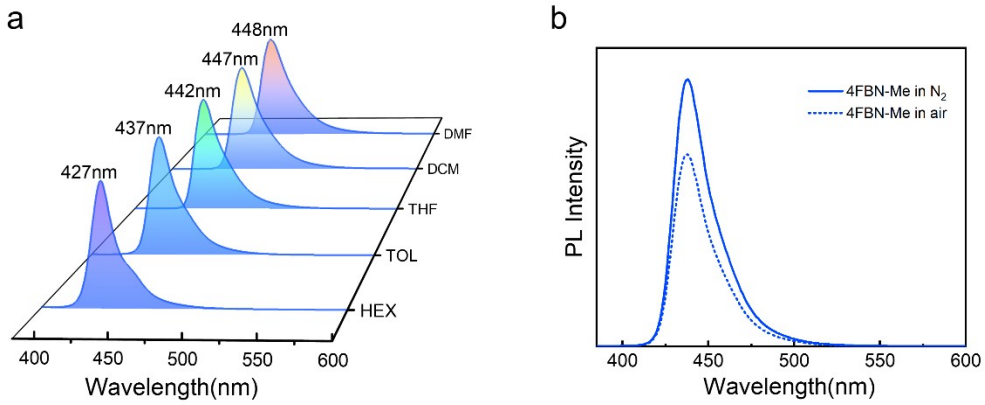

Fig. S10 (a) Solvent-dependent photoluminescence (PL) spectra of 4FBN-Me recorded in solvents with different polarities (hexane (HEX), toluene (TOL), tetrahydrofuran (THF), dichloromethane (DCM) and N,N-dimethylformamide (DMF)), showing a modest solvatochromic shift of the emission maximum. (b) PL spectra of 4FBN-Me in toluene measured under air and N_2, showing enhanced emission intensity after deoxygenation (λ_{ex} = 385 nm).

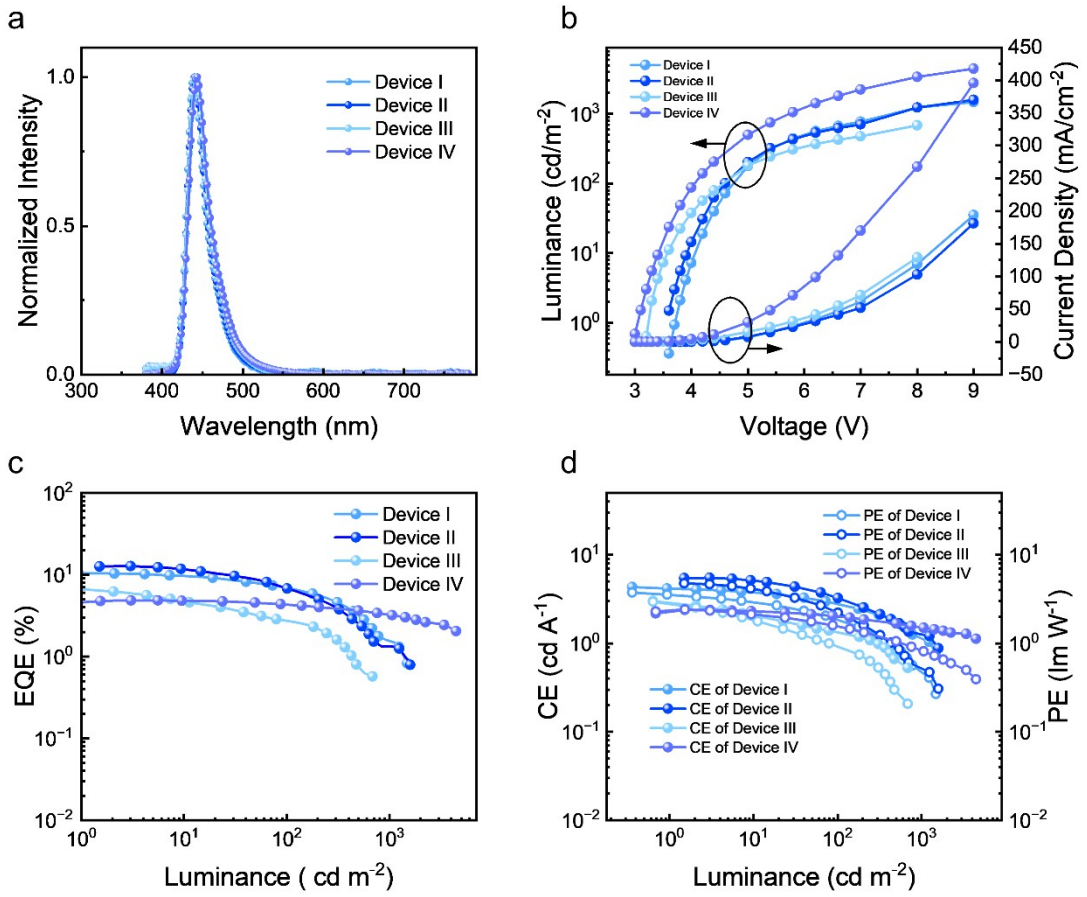

Fig. S11 Device performance summary: (a) Normalized electroluminescence (EL) spectra of Devices I–IV. (b) Current density–voltage–luminance (J–V–L) characteristics of Devices I–IV. (c) External quantum efficiency (EQE) as a function of luminance for Devices I–IV. (d) Current efficiency (CE) and power efficiency (PE) versus luminance for Devices I–IV.

Note S1 Triplet-Triplet Annihilation (TTA) Model Analysis

In general, the efficiency roll-off in OLEDs based on delayed fluorescence or phosphorescence is primarily attributed to exciton quenching processes, particularly triplet–triplet annihilation (TTA), owing to the relatively long lifetime of the excited triplet states. To quantify the efficiency roll-off, the TTA model was employed using the following equation:

$$\frac{\eta}{\eta_0} = \frac{J_0}{4J}\left(\sqrt{1+\frac{8J}{J_0}} - 1\right)$$

where η is the external quantum efficiency (EQE) in the presence of TTA, η_0 is the initial EQE in the absence of TTA (at low current density), J is the current density, and J_0 is the critical current density at which the EQE drops to half of its initial value ($\eta = \eta_0 / 2$). A larger J_0 value represents a smaller efficiency roll-off.[5, 6]

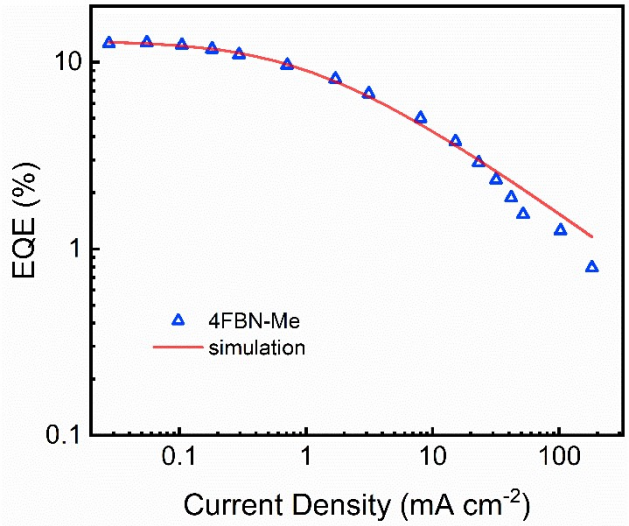

Fig. S12 EQE versus current density characteristics of the 4FBN-Me-based device. The open blue triangles represent the experimental data, and the solid red line represents the simulated EQE by employing the TTA model. The fitted critical current density (J_0) is 3.13 mA cm^{-2}, with a correlation coefficient (R^2) of 0.995, indicating that the efficiency roll-off is predominantly caused by the triplet-triplet annihilation (TTA) process.

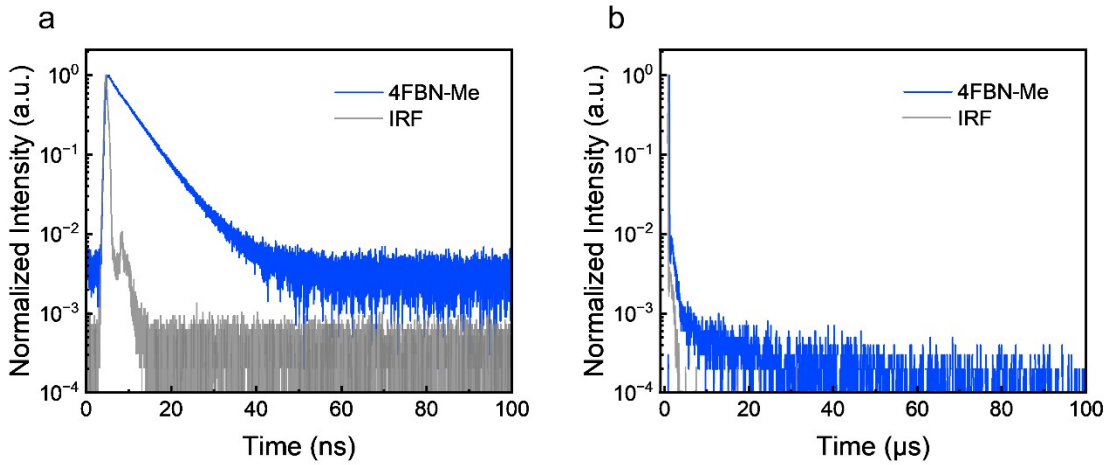

Fig. S13 Normalized transient photoluminescence decay curves of the 4FBN-Me doped film at 300 K along with the corresponding instrument response function (IRF) measured on (a) a nanosecond timescale and (b) a microsecond timescale.

Table. S2 Summary of CIE y coordinates, reverse intersystem crossing rates, and critical borylation yields for 4FBN-Me (this work) and representative deep-blue MR-TADF emitters (CIE y ≤ 0.05) reported in the literature.

Emitter	CIE y	k_{RISC} (10^4)	Borylation Yield[a] (%)
BOBO-Z[7]	0.04	7	20
DB[8]	0.048	13	60
(M)-DB-O[8]	0.041	18	53
(P)-DB-O[8]	0.041	18	53
(M)-DB-S[8]	0.047	19	31
(P)-DB-S[8]	0.048	19	31
5Cz-BO[9]	0.046	27	40
Py-BN[10]	0.045	0.64	26
Pm-BN[10]	0.045	0.42	29
DOB2-DABNA-A[11]	0.049	112	24
DPA-B3[12]	0.043	40	39
DPA-B4[12]	0.05	229	54
iPrAuBN[13]	0.036	83.4	78
2FPAB[14]	0.044	2.46	76
MePAB[14]	0.046	2.37	87
[B-N]N2[15]	0.046	0.57	95
B-O-dpa[16]	0.05	0.83	42.5
CzBO[17]	0.05	0.9	28
BIC-mCz[18]	0.05	0.4	35
mDBIC[18]	0.05	0.5	29
4FBM-Me	0.04	23.2	71

[a] Borylation yield refers to the chemical yield of the final critical step to construct the MR skeleton, which is typically the most challenging part of the synthesis.

Supplementary References

1. T. Nakagawa, S. Y. Ku, K. T. Wong and C. Adachi, *Chem. Commun.*, 2012, **48**, 9580–9582.
2. Y. Tsuchiya, S. Diesing, F. Bencheikh, Y. Wada, P. L. Dos Santos, H. Kaji, E. Zysman-Colman, I. D. W. Samuel and C. Adachi, *J. Phys. Chem. A*, 2021, **125**, 8074–8089.
3. Q. Zhang, B. Li, S. Huang, H. Nomura, H. Tanaka and C. Adachi, *Nat. Photonics*, 2014, **8**, 326–332.
4. K. Masui, H. Nakanotani and C. Adachi, *Org. Electron.*, 2013, **14**, 2721–2726.
5. M. A. Baldo, C. Adachi and S. R. Forrest, *Phys. Rev. B*, 2000, **62**, 10967–10977.
6. G. Xie, X. Li, D. Chen, Z. Wang, X. Cai, D. Chen, Y. Li, K. Liu, Y. Cao and S.-J. Su, *Adv. Mater.*, 2016, **28**, 181–187.
7. I. S. Park, M. Yang, H. Shibata, N. Amanokura and T. Yasuda, *Adv. Mater.*, 2022, **34**, e2107951.
8. Z. Ye, H. Wu, Y. Xu, T. Hua, G. Chen, Z. Chen, X. Yin, M. Huang, K. Xu, X. Song, Z. Huang, X. Lv, J. Miao, X. Cao and C. Yang, *Adv. Mater.*, 2024, **36**, e2308314.
9. R. Z. An, Y. Sun, H. Y. Chen, Y. Liu, A. Privitera, W. K. Myers, T. K. Ronson, A. J. Gillett, N. C. Greenham and L. S. Cui, *Adv. Mater.*, 2024, **36**, e2313602.
10. X. Cai, Y. Pan, C. Li, L. Li, Y. Pu, Y. Wu and Y. Wang, *Angew. Chem. Int. Ed. Engl.*, 2024, **63**, e202408522.
11. J. Ochi, Y. Yamasaki, K. Tanaka, Y. Kondo, K. Isayama, S. Oda, M. Kondo and T. Hatakeyama, *Nat. Commun.*, 2024, **15**, 2361.
12. T. Hua, X. Cao, J. Miao, X. Yin, Z. Chen, Z. Huang and C. Yang, *Nat. Photonics*, 2024, **18**, 1161–1169.
13. X. F. Song, S. Luo, N. Li, X. Wan, J. Miao, Y. Zou, K. Li and C. Yang, *Angew. Chem. Int. Ed. Engl.*, 2025, **64**, e202413536.
14. H. Su, Y. Wang, K. Di, H. Yue, S. Huang, Y. Tian, Q. Zhang, H. Shao, R. Guo and L. Wang, *Adv. Funct. Mater.*, 2024, **35**, 2414757.
15. D. Wan, J. Zhou, Y. Yang, G. Meng, D. Zhang, L. Duan and J. Ding, *Adv. Mater.*, 2024, **36**, e2409706.
16. J. Park, J. Lim, J. H. Lee, B. Jang, J. H. Han, S. S. Yoon and J. Y. Lee, *ACS Appl Mater Interfaces*, 2021, **13**, 45798–45805.
17. I. S. Park, H. Min and T. Yasuda, *Angew. Chem. Int. Ed. Engl.*, 2022, **61**, e202205684.
18. X. Wang, Y. Zhang, H. Dai, G. Li, M. Liu, G. Meng, X. Zeng, T. Huang, L. Wang, Q. Peng, D. Yang, D. Ma, D. Zhang and L. Duan, *Angew. Chem. Int. Ed. Engl.*, 2022, **61**, e202206916.